Astron. Astrophys. 332, 251–267 (1998)

ASTRONOMY AND ASTROPHYSICS

Radio observations of stellar winds from early type stars⋆,⋆⋆

S. Scuderi[1], **N. Panagia**[2,3], **C. Stanghellini**[4], **C. Trigilio**[4], **and G. Umana**[4]

[1] Osservatorio Astrofisico di Catania, Viale Andrea Doria 6, I-95125 Catania, Italy (e-mail: scuderi@ct.astro.it)
[2] Space Telescope Science Institute, 3700 San Martin Drive, Baltimore, MD 21218, USA (e-mail: panagia@stsci.edu)
[3] Affiliated to the Astrophysics Division, Space Science Department of ESA
[4] Istituto di Radioastronomia del CNR, Stazione VLBI di Noto, C.P. 141, I-96017 Noto, Italy
(e-mail: carlo@ira.noto.cnr.it, umana@ira.noto.cnr.it, trigilio@ira.noto.cnr.it)

Received 20 May 1997 / Accepted 18 November 1997

Abstract. Fifteen O and B supergiants have been observed with the Very Large Array (VLA) at 4.85, 8.45, and 14.95 GHz in order to make a detailed comparative study of the mass loss rates evaluated from Hα and radio continuum observations and reveal and quantify possible departures from standard wind conditions. We detected 12 sources, 7 of which for the first time, thus increasing by 30% the total number of detections of OB supergiants in the northern sky. Radio spectral slopes indicate that the radio emission is mainly of thermal origin in all objects with one exception (HD 190603) out of the 12 detections. Our results demonstrate the value of using Hα for mass loss rate determinations, especially for stars that are too distant or too faint to be detected with radio techniques. The relationship $\dot{M} - L$ for supergiants turns out to be appreciably flatter than commonly reported, *i.e.* $\log \dot{M} = (1.25 \pm 0.30) \log L$.

Key words: stars: early-type – stars: mass loss – stars: supergiants – radio continuum: stars

1. Introduction

Stellar winds play an essential role in the physics of the stars and the interstellar medium. In fact, the evolution of a star is strongly affected by mass evaporation induced by stellar winds ($e.g.$ Chiosi & Maeder 1986). Furthermore, the continuous deposition of mass, momentum, and energy in the interstellar medium produces important effects on its physical and dynamical properties and on its evolution ($e.g.$ Abbott 1982, Leitherer et al. 1992).

Early type stars are observed to have very strong stellar winds. The most common diagnostic tools to obtain information on the wind properties are based on a) the analysis of UV lines, b) the study of the IR and radio continuum emission, and c) the analysis of the hydrogen emission lines, most commonly the Hα line. The parameters that can be determined are the mass loss rate, the velocity (and hence the density) radial distribution, the temperature and the chemical composition of winds.

Some of these diagnostic tools depend heavily on *a priori* assumptions, which make the results of the analysis not quite reliable. In particular, UV lines are produced by ions whose degrees of ionization are not directly measured and have to be inferred through ponderous as well as uncertain modelling (see, for example, Lamers 1988). The infrared thermal emission is very sensitive to the density structure of the inner parts of the wind where it is formed but which cannot be determined from the observations themselves ($e.g.$ Simon & Castor 1983).

On the other hand, the study of the radio emission and the analysis of the Hα line can provide much more accurate and reliable information on the stellar wind properties.

Radio observations, in principle, should provide the most reliable method for determining the mass loss rate from an early type star as long as the emission is of thermal origin, i.e. free-free radiation produced in the outer parts of the wind. In this case the measured flux is simply related to the mass loss rate and the expansion velocity and the interpretation of the radio measurements is straightforward (Panagia & Felli 1975; Wright & Barlow 1975). Therefore the mass loss determination should be free of uncertain assumptions and systematic effects which, to different extents, affect all other types of analysis. However, although several tens of objects have been observed so far, due to their low flux densities, only about twenty stars have accurate flux density determinations (Bieging et al. 1989 and references therein; Howarth & Brown 1991 for the northern hemisphere; Leitherer et al. 1995 for the southern hemisphere). Another complication arises from the fact that part of the emission is of non-thermal origin. Actually, non-thermal emission appears

⋆ Based on observations with the Very Large Array. The VLA is a facility of the National Radio Astronomy Observatory which is operated by the Associated Universities Inc. under cooperative agreement with the National Science Foundation.

⋆⋆ This research has made use of the Simbad database, operated at CDS, Strasbourg, France

Table 1. Stellar and wind parameters[a]

Object	ST	T_{eff} [10^4 K]	v_∞ [km s$^-$1]	$\dot{M}$(Hα) [10^{-6} M$_\odot$ yr^{-1}]	d [kpc]	R [R$_\odot$]	S_ν(8.45GHz) predicted [mJy]
HD 190429	O4If	4.24	1880	7.5	1.7	17	0.50
HD 14947	O5If	4.03	1885	5.4	2.0	15	0.23
HD 192639	O7Ibf	3.61	2180	2.4	1.3	13	0.15
HD 30614 – $\alpha\ Cam$	O9.5I	3.09	1590	2.9	1.0	26	0.50
HD 195592	O9.5I	3.09	(1765)	3.8	1.3	30	0.37
HD 37128 – $\epsilon\ Ori$	B0Ia	2.60	1910	1.6	0.5	33	0.75
HD 2905 – $\kappa\ Cas$	B1Ia	2.08	1105	1.1	1.1	41	0.18
HD 193237 – $P\ Cyg$	B1Ia$^+$	1.93	210	19.0	2.0	76	9.62
HD 190603	B1.5Ia	1.96	485	3.5	1.5	52	1.31
HD 194279	B1.5Ia	1.96	(750)	1.5	1.0	41	0.54
BD -14 5037	B1.5Ia	1.96	(750)	3.4	1.7	54	0.55
HD 41117	B2Ia	1.85	510	1.6	1.5	58	0.43
HD 198478	B3Ia	1.62	470	0.5	0.8	37	0.35
Cyg OB2 12	B5Ia	1.36	(500)	8.6	1.8	228	2.81
HD 208501	B8Ib	1.12	(500)	0.7	0.7	55	0.64

[a] See text for explanation.

to dominate the radio spectrum of about 30% of all early type stars (Bieging et al. 1989, hereafter referred to as BAC 1989).

Hydrogen lines are not much affected by uncertainties in the chemical composition and the ionization equilibrium of the wind. Moreover, even if they are formed in the inner regions of the wind, as is for the IR continuum, their profiles convey all the information regarding the structure of the emitting layers (velocity and density distributions), so that a fit of the line profiles allows one to derive simultaneously the global parameters of the wind, such as the mass loss rate, and the density structure of the outflowing material. The great potential of this approach has been already shown by several different authors (Olson & Ebbets 1981; Ebbets 1982; Scuderi et al. 1992, 1994; Puls et al. 1996).

Within this framework we have started a project to study a statistically significant sample of early type stars through observations both in Hα and in the radio. It is worthwhile to note that, since the last radio survey of early type stars (BAC 1989), the VLA capabilities have greatly improved, especially at 8.45 GHz (3.5 cm). The analysis of this sample will provide a fundamental consistency check for the two methods. This is particularly important for an ideal use of the Hα method every time the radio cannot give useful information ($e.g.$ strong non thermal contribution, or flux density too low because of either a low mass loss rate or a far distance). Furthermore, since radio and Hα emission originate from different parts of the wind, the two independent determinations of the mass loss will provide valuable information about the detailed structure and the symmetry of the expanding envelope (clumping, beaming, etc.).

Sect. 2 describes the sample selection, the observations and the data reduction. In Sect. 3 we give a brief overview of the basics of emission by stellar winds from early type stars. Sect. 4 is devoted to the analysis of the observations with comments on individual stars. Finally, in Sect. 5 we discuss the results obtained in terms of the general properties of radio emission ($i.e$, origin of the emission, variability etc.) and the correlation of the radio emission with the stellar parameters.

2. Observations

2.1. The sample selection

In 1988 we started at Catania Astrophysical Observatory (CAO) a program of systematic spectroscopic ($R \sim 7000$) observations of the Hα line of O and B type supergiants. The target sample consists of all O and B type supergiants accessible from the northern sky at CAO and brighter than 11th mag (in V). So far we have observed 35 out of about 60 program stars. We have developed a model (Scuderi et al. 1992, 1994) to calculate theoretical Hα profiles to fit the observations (see also Sect. 3.1). Using this model we have derived the properties of the winds (mass loss rate and velocity field) of these objects (Scuderi et al. 1992, 1994; Scuderi 1994; Scuderi & Panagia 1997).

Once the mass loss rate and the velocity field are determined one can estimate (see Sect. 3.1.1) the expected emission of the wind at radio wavelengths. We calculated the expected radio emission for the objects of the whole sample and selected for radio observations a subset whose expected fluxes were within the present VLA capabilities.

Table 1 shows the list of the program stars together with the adopted stellar parameters, the wind parameters and the predicted radio flux at 8.45 GHz (the predicted radio fluxes at 14.95 and 4.85 GHz can be obtained multiplying the 8.45 GHz flux by 1.4 and 0.73 respectively). The spectral types are as listed by Leitherer (1988) and the SIMBAD database. The effective temperatures, T_{eff}, of the O supergiants are from Chlebowski

& Garmany (1991) calibration, whereas the temperatures of the B supergiants are from Schmidt–Kaler (1982) calibration. Distances, d, are from Humphreys (1978) and Garmany & Stencel (1992). Stellar radii, R, were obtained from effective temperatures and luminosities. The mass loss rate is the one derived from the Hα analysis and the terminal velocities, v_∞, are those measured by Prinja et al. (1990) for all objects except $P\ Cygni$ for which we adopted the terminal velocity has been derived by Lamers et al. (1985). The values in parentheses are not measurements but correspond to the average value of v_∞ of objects having the same spectral type and luminosity class as the object in the sample.

Table 2. Previously Detected Objects

Object	S_ν[mJy]		Ref.
	14.95GHz	4.85GHz	
HD 30614 – $\alpha\ Cam$	–	0.35±0.07	3
HD 37128 – $\epsilon\ Ori$	–	1.6±0.5	2
HD 190603	1.0±0.3	0.6±0.2	1,2
HD 193237 – $P\ Cyg$	16.6±0.5	6.7±0.2	3,4
Cyg OB2 12	6.0±2.0	2.9±0.2	3

[1] Abbott (1980).
[2] Abbott, Bieging, Churchwell, & Cassinelli (1985).
[3] Bieging, Abbott, Churchwell (1989).
[4] van den Oord et al. (1985).

2.2. Observations and data reduction

The observations were carried out with the VLA in two sessions of twelve hours each in moving configuration. The first session was between September 12 and September 13, 1994 with the $B \rightarrow CnB$ moving configuration and the second run a month later between October 13 and October 14, 1994 in the $CnB \rightarrow C$ configuration. In both epochs 3 to 6 antennas, mostly the inner ones, were completely or partially missing due to the reconfiguration of the array.

The 3 objects with the weakest predicted fluxes were observed at 8.45 GHz only, where sensitivity is highest. With regard to the other objects, 9 stars were observed at three frequencies, 14.95, 8.45, and 4.85 GHz, and the remaining 3 at 8.45 and 4.85 GHz. All the frequencies had a 100 MHz bandwidth.

The Astronomical Image Processing System (AIPS) developed by the National Radio Astronomy Observatory (NRAO) has been used for editing, calibrating and imaging the data. Flux densities were tied to the flux density of the radio sources 3C286 and 3C48 using the modified scale of Baars et al. (1977) implemented in AIPS. The flux densities for 3C48 were taken to be 1.81, 3.23 and 5.53 Jy at 14.95, 8.45 and 4.85 GHz respectively, while for 3C286 were 3.43, 5.19 and 7.50 Jy. A phase calibrator was observed for 1-2 minutes before and after each scan of typically 10 minutes. In each session at least two scans at different hour angles were observed for each object. The data have been imaged with a natural UV weighting to maximize the sensitivity and deconvolved using the Cotton-Schwab algorithm as implemented in AIPS (Cornwell & Braun 1994).

One problem occurring during reconfiguration is that the positions of the moved antennas are poorly determined, resulting in large phase errors in the visibility data, especially at higher frequencies. If the SNR is high enough, self calibration can remove the first order effects of the phase errors. This was not possible for such detection experiment. However, the accurate positions of the antennas were given $a\ posteriori$ and it was possible to apply the corrections during the data reduction. This has been done with evident improvement of the image quality as the images of the detected sources show. Some residual errors due to this effect may still be present but we are confident that the fluxes obtained are reliable within the quoted errors.

The radio sources 3C286 and 3C48 used as primary calibrators are partially resolved for most frequencies and configurations at the VLA and the amplitude gains of the single antennas need to be calculated using only the short baselines. The problem is more severe at higher frequencies and at 15 GHz it is necessary to use only the inner antennas of the array which were absent or malfunctioning in our observations.

Ignoring the guidelines and blindly calibrate the data on the basis of the available data introduces a flux error not exceeding 5% as mentioned in the VLA calibrator manual. To be very conservative we considered a 15 % error for our 15 GHz data.

We detected 12 sources, 7 of which had never been detected before. We were able to detect at all frequencies the sources previously detected (see Table 2) as well as three of the newly detected stars. One object was detected at 8.45 GHz and 4.85 GHz, three objects were detected only at 8.45 GHz, and the three remaining objects were not detected at any observed frequency. Some sources ($Cyg\ OB2$ 12 and $P\ Cygni$) seem to be resolved in our images but due to the remaining phase errors we cannot exclude that it is an instrumental effect.

The selected sample includes 10 stars which had never detected or observed in the radio before, and 5 stars which had already been detected at one frequency at least. Table 2 summarizes the fluxes for these objects available from the literature.

Table 3 displays the log of the observations, the integration times for each source, the measured flux densities at 14.95, 8.45, and 4.85 GHz together with the 1σ r.m.s. noises for the detections and the 3σ upper limit for the non-detections. The error on the flux density is given by the combination of the r.m.s. noise and of the calibration errors, i.e.

$$\sigma = \sqrt{(rms)^2 + (aS)^2}$$

where S is the measured flux density and a is the relative error on the flux calibration and it is equal to 0.03 for the 4.85 and 8.45 GHz measurements and to 0.15 for the 14.95 GHz measurements. The larger calibration error in the 14.95 GHz data is due to the problems in determining good solutions for the flux density of the primary calibrators as discussed above. In Figs. 1-10 the contour maps of the radio emission at 14.95, 8.45, and 4.85 GHz for all the detected objects are shown.

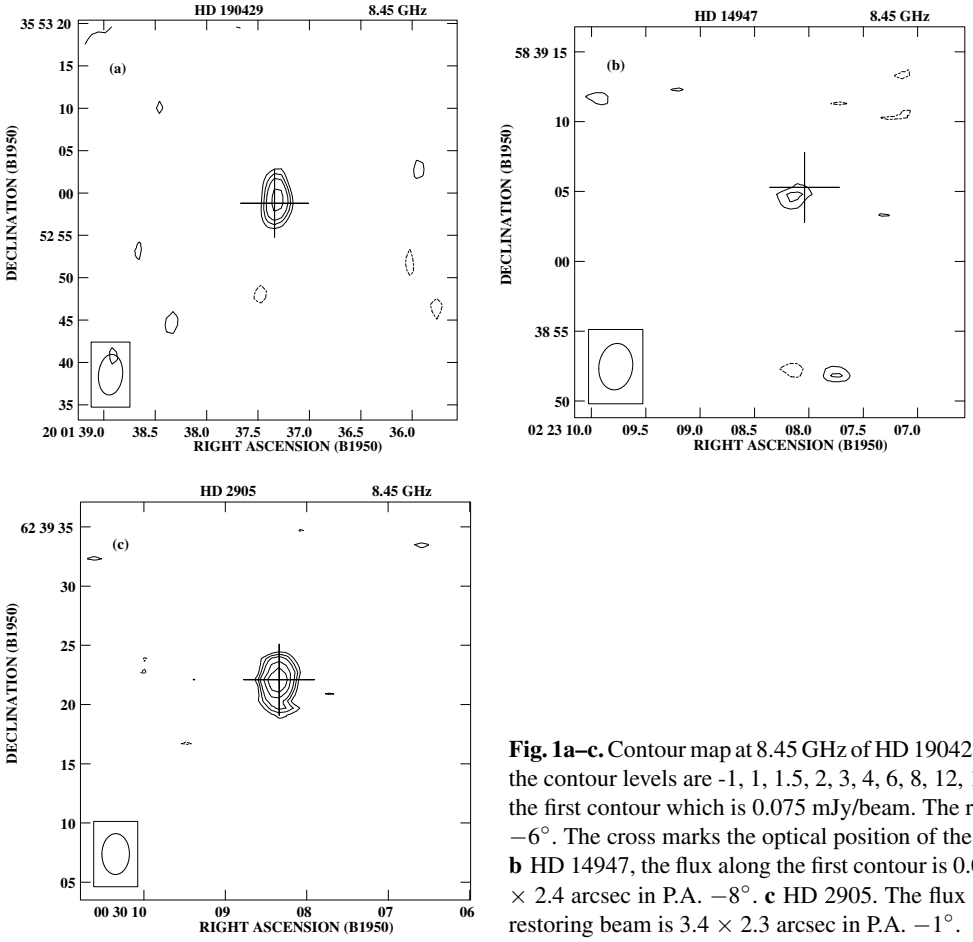

Fig. 1a–c. Contour map at 8.45 GHz of HD 190429, HD 14947 and HD2905. **a** HD 190429, the contour levels are -1, 1, 1.5, 2, 3, 4, 6, 8, 12, 16, 25, 35, 50, 70, 100.0 $\times$ the flux along the first contour which is 0.075 mJy/beam. The restoring beam is 4.8 $\times$ 2.8 arcsec in P.A. -6°. The cross marks the optical position of the star obtained from the Simbad database. **b** HD 14947, the flux along the first contour is 0.075 mJy/beam. The restoring beam is 3.3 $\times$ 2.4 arcsec in P.A. -8°. **c** HD 2905. The flux along the first contour is 0.075 mJy. The restoring beam is 3.4 $\times$ 2.3 arcsec in P.A. -1°.

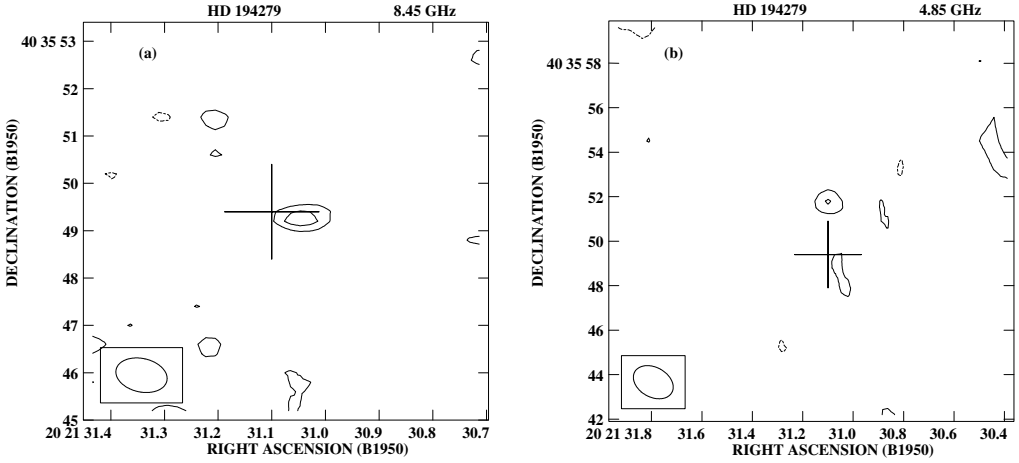

Fig. 2a and b. Contour maps at 8.45 **a**, 4.85 **b** GHz of HD 194279. **a** The flux along the first contour is 0.25 mJy/beam. The restoring beam is 1.1 $\times$ 0.7 arcsec in P.A. +78°. **b** The flux along the first contour is 0.20 mJy/beam. The restoring beam is 1.9 $\times$ 1.3 arcsec in P.A. +61°.

3. Emission from stellar winds

3.1. Brief overview

In this section we briefly describe the wind model used for the interpretation of the Hα and radio observations.

3.1.1. Basic equations

As usual we assume that the wind is stationary, spherically symmetric, fully ionized, and isothermal. In addition, for the velocity field we assume a truncated power-law dependence with radius (Panagia 1991).

$$v = v_\circ \left(\frac{r}{R}\right)^\gamma \qquad r \leq R_1 = R\left(\frac{v_\infty}{v_\circ}\right)^{1/\gamma} \tag{1}$$

$$v = v_\infty \qquad r \geq R_1 \tag{2}$$

where $v_\circ$ and v_∞ are the initial (at the base of the wind) and the terminal velocities of the wind respectively and R is the stellar radius. The model calculation of the Hα profiles includes: i) the

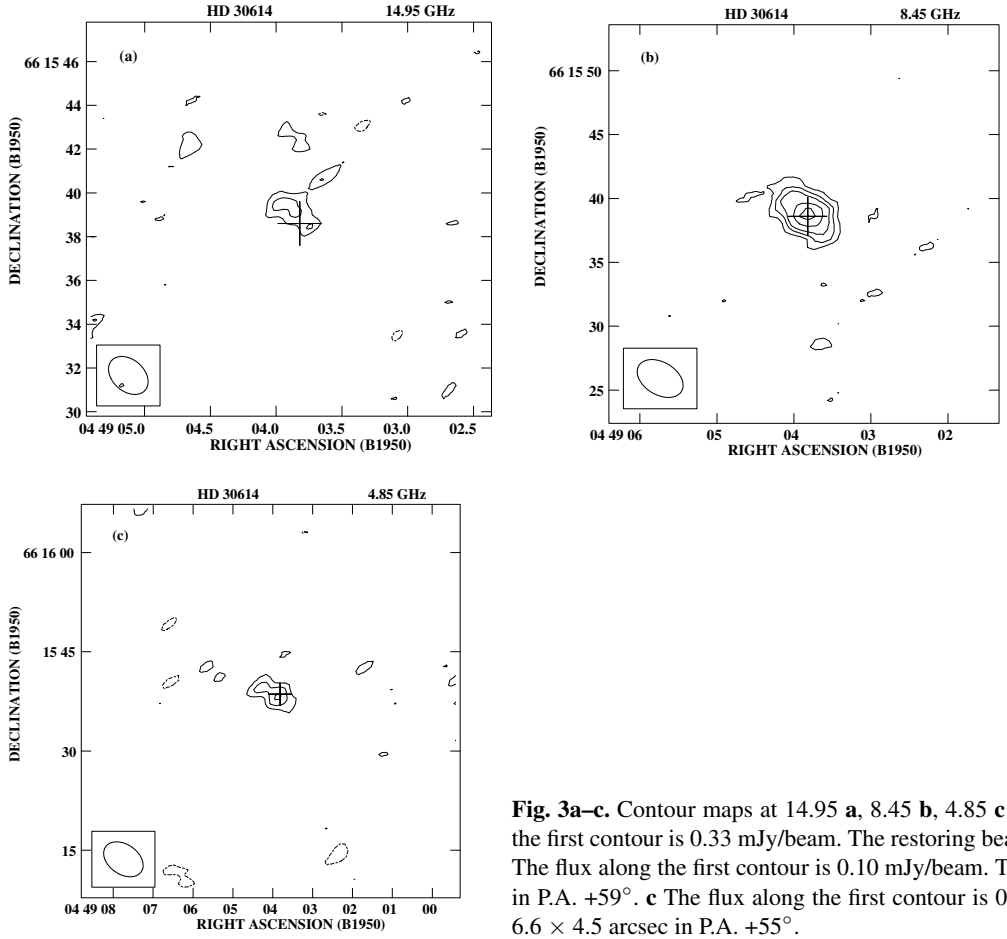

Fig. 3a–c. Contour maps at 14.95 **a**, 8.45 **b**, 4.85 **c** GHz of HD 30614. **a** The flux along the first contour is 0.33 mJy/beam. The restoring beam is 2.1 × 1.5 arcsec in P.A. +49°. **b** The flux along the first contour is 0.10 mJy/beam. The restoring beam is 3.9 × 2.6 arcsec in P.A. +59°. **c** The flux along the first contour is 0.12 mJy/beam. The restoring beam is 6.6 × 4.5 arcsec in P.A. +55°.

effects of photospheric absorption, ii) scattering and iii) emission by hydrogen atoms as well as the effects of iv) electron scattering, whenever it turns out to be important ($cf.$ Scuderi et al. 1994). The Hα radiative transfer is treated in the Sobolev approximation. By fitting an observed profile with model calculations one can determine the mass loss rate, $\dot{M}$, and the velocity field, in terms of the initial velocity, $v_\circ$, and the exponent of the power law, γ. In addition, the electron temperature can also be determined when the electron scattering line wings can be measured. In particular, the mass loss rate is given by

$$\dot{M} = 0.203\mu_e \left(\frac{\tau_\circ}{b_2}\right)^{1/2} \left[\frac{R}{10R_\odot}\right]^{3/2} \left[\frac{v_\circ}{100km\ s^{-1}}\right]^{3/2} \times \left[\frac{T_e}{10^4K}\right]^{3/4} \left[e^{E_2/kT} - e^{E_3/kT}\right]^{-1/2} 10^{-6}\ \mathrm{M_\odot\ yr^{-1}} \quad (3)$$

where the optical depth at the center of the Hα line, $\tau_\circ$, and the initial velocity $v_\circ$ are obtained from the profile fit, T_e, the electron temperature, in general, is assumed to be equal to $0.85 \times T_{eff}$. The quantity μ_e is the mean atomic weight per free electron, set equal to 1.3 for a fully ionized gas composed of 90% hydrogen and 10% helium. E_2 (3.39 eV) and E_3 (1.51 eV) are the ionization energies from the second and the third level of hydrogen, respectively, and b_2 is the ratio of the population of the second level to that in LTE. In our calculations we adopted an average value of b_2 = 1.3 for the O supergiants (Klein & Castor 1978), and b_2 = 3 for the B supergiants (Lamers, private communication).

The interpretation of the radio data is more straightforward. The main emission mechanism is free-free radiation. The transfer equation is solved taking into account the fact that the radio photosphere is located at several stellar radii from the surface of the star where the expanding envelope approaches its terminal velocity so as the outflow is well approximated by a constant velocity density distribution. The basic model for the continuum wind emission was developed by Panagia & Felli (1975) and Wright & Barlow (1975). They showed that the emitted radio flux can be related to the mass loss rate as follows

$$S_\nu = 7.26 \left[\frac{\nu}{10GHz}\right]^{0.6} \left[\frac{T_e}{10^4K}\right]^{0.1} \left[\frac{\dot{M}}{10^{-6}M_\odot yr^{-1}}\right]^{4/3} \left[\frac{\mu_e v_\infty}{100km\ s^{-1}}\right]^{-4/3} \left[\frac{d}{kpc}\right]^{-2} \mathrm{mJy} \quad (4)$$

where d is the distance and all the other quantities have already been defined.

3.1.2. Dependence on the distance and the stellar radius

We would like to note that the Hα mass loss rate is only *apparently* independent of the distance. Actually, the distance of

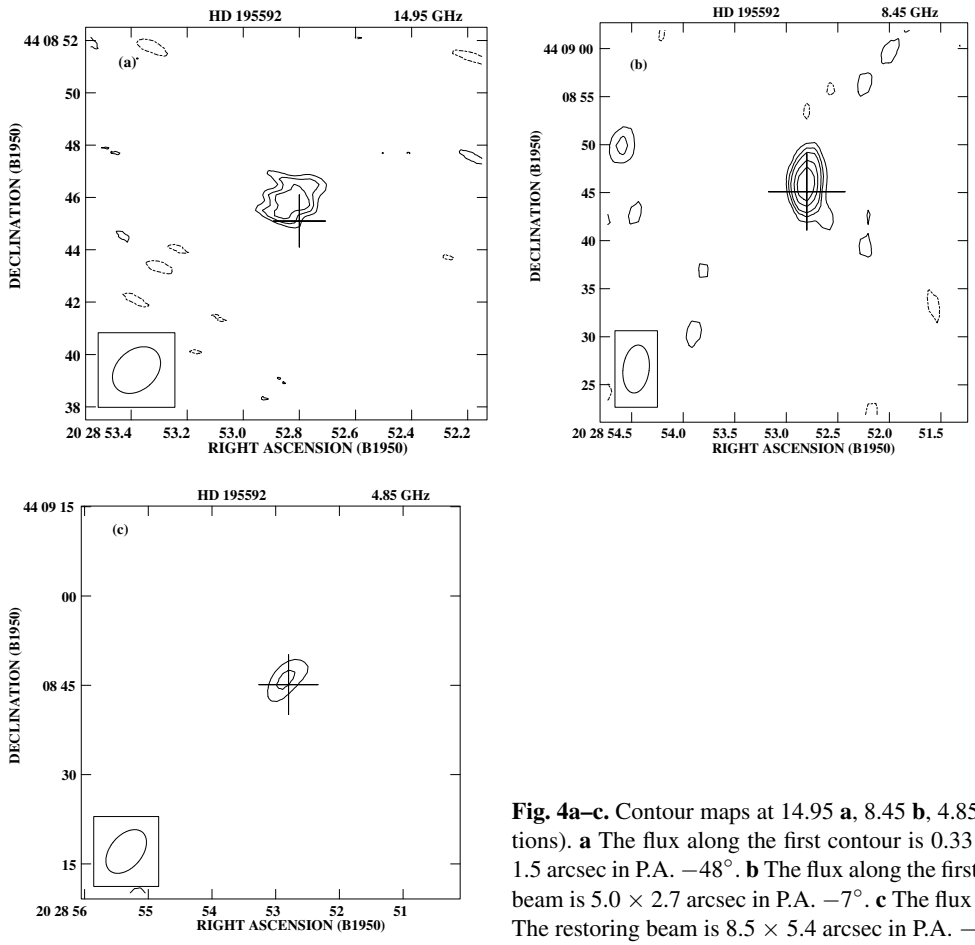

Fig. 4a–c. Contour maps at 14.95 **a**, 8.45 **b**, 4.85 **c** GHz of HD 195592 (october observations). **a** The flux along the first contour is 0.33 mJy/beam. The restoring beam is 2.1 × 1.5 arcsec in P.A. -48°. **b** The flux along the first contour is 0.10 mJy/beam. The restoring beam is 5.0 × 2.7 arcsec in P.A. -7°. **c** The flux along the first contour is 0.18 mJy/beam. The restoring beam is 8.5 × 5.4 arcsec in P.A. -40°.

a star enters implicitly through the value of the stellar radius. In fact, the stellar radius is calculated through the luminosity, and hence the distance, of the star once its spectral type ($i.e.$ its effective temperature) is known. In particular $R \propto d$, and this yields a $\dot{M}(H\alpha) \propto d^{3/2}$ functional dependence. From Eq. (4) turns out that the radio mass loss rate has the same functional dependence on the distance $i.e.$ $\dot{M}(radio) \propto d^{3/2}$. Therefore, the ratio of the mass loss rates determined from the Hα profile fitting and from radio observations is independent of the distance. This means that the estimate of the radio flux through Eq. (4), adopting the Hα mass loss rate is independent of the knowledge of the distance.

3.2. Hα and radio emission in the general case

In general, there are a number of factors that may influence the emission from a stellar wind so as to affect the interpretation of the measurements at different wavelengths (Panagia 1991), such as incomplete ionization, departure from spherical symmetry, non-thermal emission, etc. In the following we summarize them briefly.

3.2.1. Incomplete ionization

Of the two scenarios examined by Panagia (1991) i.e. a) ionization bounded wind and b) incomplete ionization throughout the wind, only the first one is relevant to our case. The wind is fully ionized up to a certain radius and becomes mostly neutral beyond that: this is the analog to a Strömgren sphere for the case of an outflow. This problem has been studied in detail by Felli & Panagia (1982) and Simon et al. (1983) who have shown that if such a situation occurs at all, the boundary is likely to be very close to the base of the flow. As a consequence, the radio emission, which takes place at a distance of several hundred stellar radii in the envelope, can drastically be reduced by orders of magnitude.

To have some clues about the ionization status of the wind one can compare the expected Lyman photon flux emitted by the star, $N^{\star}_{Ly}$, with that needed to keep the wind fully ionized, N^{w}_{Ly}. The number of Lyman continuum photons emitted by the star per second is

$$N^{\star}_{Ly} = 4\pi R^2 \times \int_{\nu_\circ}^{\infty} \frac{\pi F_\nu}{h\nu} d\nu \ \mathrm{s}^{-1} \qquad (5)$$

where πF_ν is the flux at the surface of the star at the frequency ν, and $\nu_\circ$ is the frequency corresponding to the ionization threshold for the hydrogen atom. On the other hand the Lyman continuum photon flux needed to keep the whole envelope fully ionized can be estimated using the results from Felli & Panagia (1982). They showed that this quantity can be related to the parameters of the

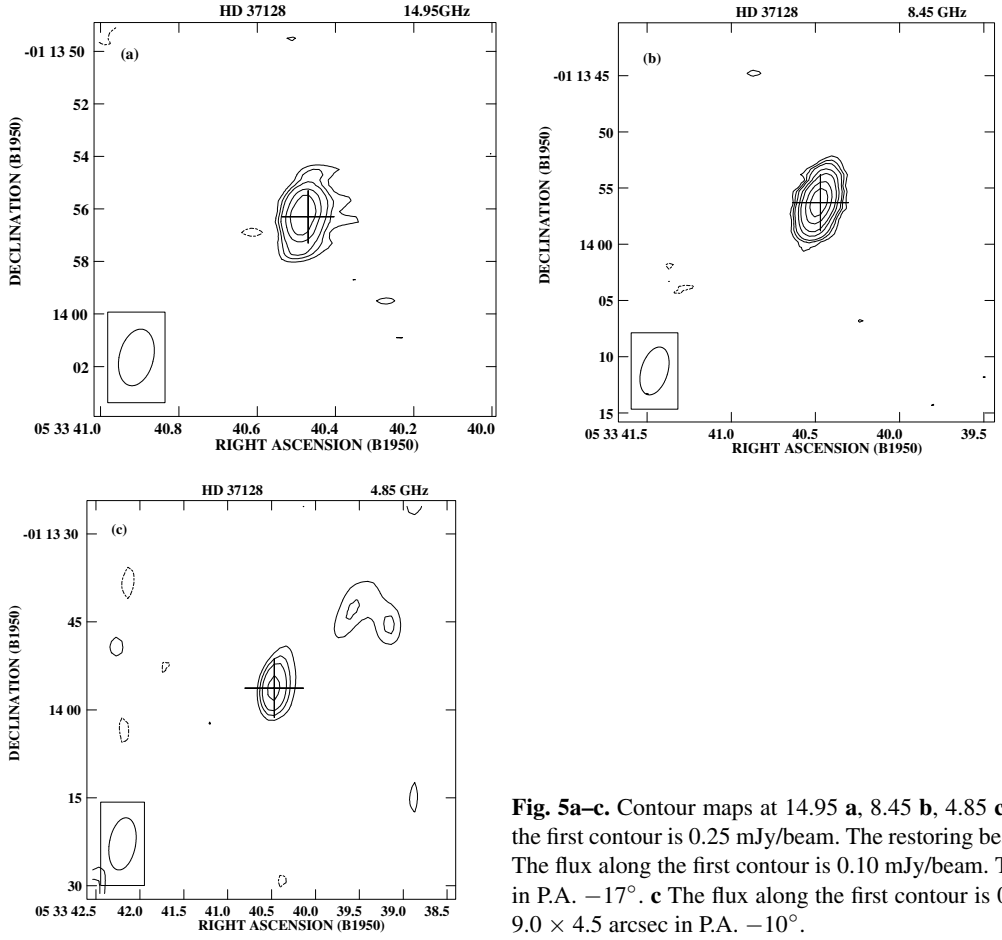

Fig. 5a–c. Contour maps at 14.95 **a**, 8.45 **b**, 4.85 **c** GHz of HD 37128. **a** The flux along the first contour is 0.25 mJy/beam. The restoring beam is 2.2×1.3 arcsec in P.A. -14°. **b** The flux along the first contour is 0.10 mJy/beam. The restoring beam is 4.4×2.4 arcsec in P.A. -17°. **c** The flux along the first contour is 0.15 mJy/beam. The restoring beam is 9.0×4.5 arcsec in P.A. -10°.

star and of the wind as follows

$$N_{Ly}^{w} = \frac{3.02 \times 10^{47}}{1+2\gamma} \left[\frac{\dot{M}}{10^{-6} M_{\odot} yr^{-1}}\right]^{2} \left[\frac{v_{\circ}}{100\ km\ s^{-1}}\right]^{-2} \times \left[\frac{R}{10\ R_{\odot}}\right]^{-1} \left[\frac{T_e}{10^4\ K}\right]^{-0.8} \left[\frac{\mu_e}{1.2}\right]^{-2} \times \left[1 + 2\gamma \left(v_{\circ}/v_{\infty}\right)^{\frac{1+2\gamma}{\gamma}}\right]\ \mathrm{s}^{-1} \quad (6)$$

It is clear that if $N_{Ly}^{w} > N_{Ly}^{\star}$ then the star has not enough Lyman continuum photons to keep the wind ionized everywhere and, in particular, in the region where the radio emission should originate.

3.2.2. Departure from spherical symmetry

The case of an outflow not spherically symmetric has been considered in detail by Schmid-Burgk (1982) and Reynolds (1986). The lack of spherical symmetry may affect both the spectral slope of the radio continuum and the absolute value of the emitted flux and hence the estimate of the mass loss rate. As for the slope of the continuum, the lack of spherical symmetry may affect it appreciably only if the fraction of solid angle filled by the flow varies systematically with the radius. As for the absolute value of the flux it is found that, irrespective of the details of the source geometry, only highly anisotropic structures can give results appreciably deviant from the predictions of the spherically symmetric models. If this happens the mass loss rate derived with spherical wind formulae may be strongly overestimated.

3.2.3. Time variability

One of the basic assumptions is that the mass loss process is steady with time. A discussion of the main effects of time variability has been presented by Felli et al. (1985). One can distinguish two cases: i) variation of the mass loss rate, and ii) variation of the ionization. In the former case one expects to detect short term variability in the optical and IR but not in the radio because, even if the $\dot{M}$ variation is instantaneous, the transit time of the front is

$$t_{transit} \simeq R_{eff}/v = 19.3 \left[\frac{R_{eff}}{10 R_{\odot}}\right] \left[\frac{v}{100 kms^{-1}}\right]^{-1}\ \mathrm{hours} \quad (7)$$

where R_{eff} is defined as the radius of a black body at the wind temperature which emits the same flux as the wind at a given frequency (see Panagia 1991), i.e. it is an estimate of the size of the emitting region at that frequency; v is the wind velocity at R_{eff}. The transit time is, therefore, of the order of a few hours in the optical but it can be of the order of weeks or months in the radio. Whether or not one sees any variation at all in the radio

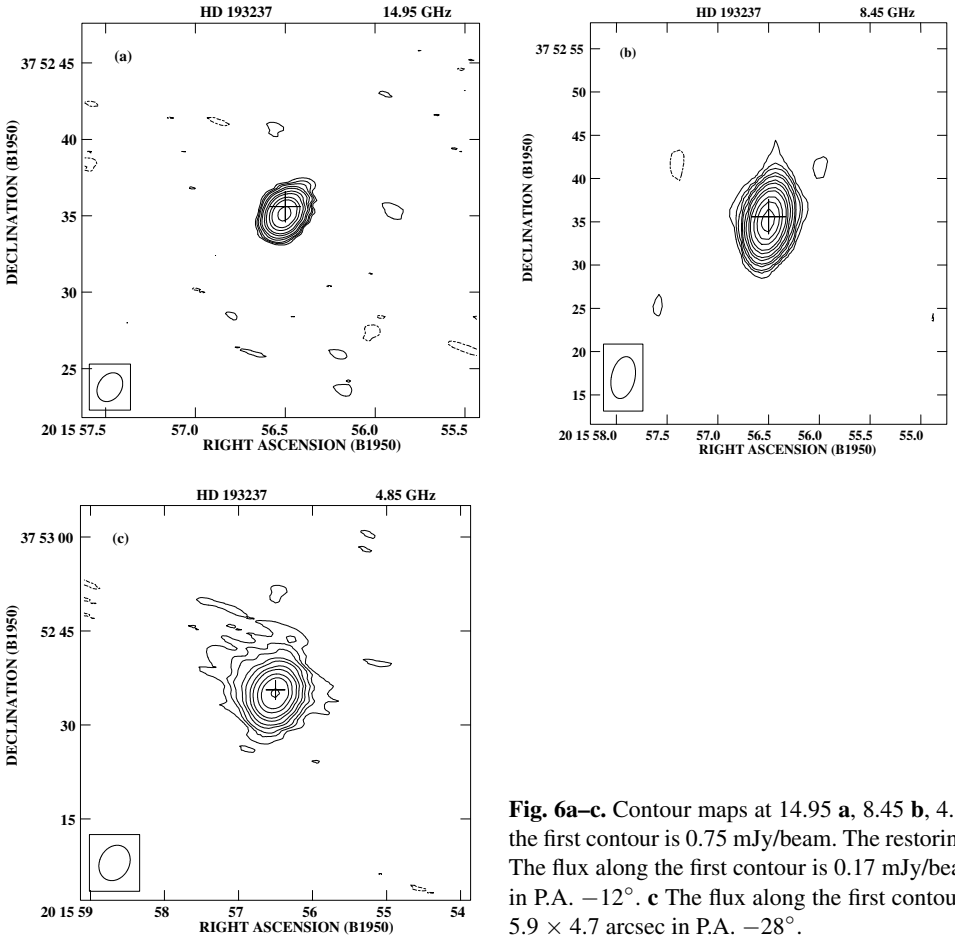

Fig. 6a–c. Contour maps at 14.95 **a**, 8.45 **b**, 4.85 **c** GHz of HD 193237. **a** The flux along the first contour is 0.75 mJy/beam. The restoring beam is 2.0×1.5 arcsec in P.A. -34°. **b** The flux along the first contour is 0.17 mJy/beam. The restoring beam is 4.9×2.7 arcsec in P.A. -12°. **c** The flux along the first contour is 0.50 mJy/beam. The restoring beam is 5.9×4.7 arcsec in P.A. -28°.

depends on the time scale of the intrinsic variation: if it occurs over a time much shorter than a few weeks, then the variations will completely be averaged out in the radio. In the case in which the ionization varies, the situation is different. Again assuming that the ionizing agent undergoes a sudden variation, the time scale of the phenomena is set by the recombination time which varies like a higher power of the radius:

$$t_{rec} = \frac{1}{n_e \beta_2} = 7.4 \left[\frac{\dot{M}}{10^{-6} M_\odot yr^{-1}}\right]^{-1} \times \left[\frac{R_{eff}}{10 R_\odot}\right]^2 \left[\frac{v}{100 kms^{-1}}\right] \left[\frac{\mu_e}{1.3}\right] \left[\frac{T}{10^4 K}\right]^{0.8} \text{seconds} \quad (8)$$

where n_e is the electron density at R_{eff} and β_2 is the recombination rate to all the excited levels of hydrogen (see Felli & Panagia 1982). Therefore, one expects a much more prompt reaction in the optical and IR, which originate in the inner and denser layers, than in the radio. These points stress the importance of making simultaneous measurements at widely different frequencies in order to understand the nature and the origin of the variability.

3.2.4. Non-thermal emission

The main non-thermal process which is relevant for early type stars is synchrotron radiation. It is produced by electrons spiraling in a magnetic field and is regarded as a non-thermal process because it is an efficient process only with energetic electrons and these are abundant enough in non-thermal situations. The main characteristics of non–thermally emitting regions are i) a typical power law spectrum which, unlike to thermal spectra, increases with wavelength, ii) high polarization iii) high brightness, and iv) short term variability. More detailed discussions on the non-thermal emission processes in early type stars stars can be found in White (1985).

4. Analysis of the observations

4.1. Non detected objects: HD 198478, HD 208501, HD 192639

We had three non detected objects two B supergiants and one O supergiant.

For the first one, HD 208501 (B8Ib), the predicted flux at 8.45 GHz (see Table 1) is 0.64 mJy. The accuracy of this estimate depends mainly on the accuracy to which the ratio $\dot{M}/v_\infty$ is known. The terminal velocity reported in Table 1 was measured by Prinja et al. (1990) with an estimated accuracy better than 20% (the error on the velocity measurements is claimed to be always $\leq$ 100 km s^{-1}). The uncertainty on the value of the mass loss rate deduced from the Hα is about 20%. So the uncertainty on the predicted radio flux is of $\sim 25\%$. This means

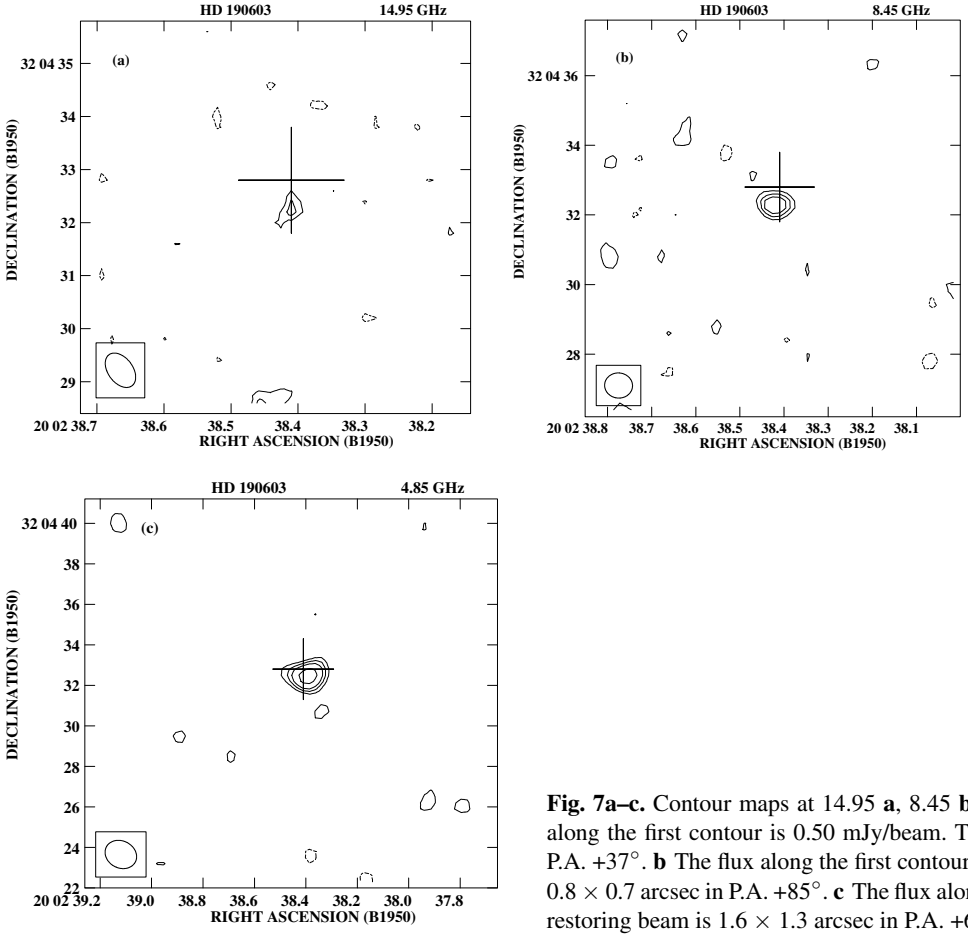

Fig. 7a–c. Contour maps at 14.95 **a**, 8.45 **b**, 4.85 **c** GHz of HD 190603. **a** The flux along the first contour is 0.50 mJy/beam. The restoring beam is 0.7 × 0.5 arcsec in P.A. +37°. **b** The flux along the first contour is 0.25 mJy/beam. The restoring beam is 0.8 × 0.7 arcsec in P.A. +85°. **c** The flux along the first contour is 0.15 mJy/beam. The restoring beam is 1.6 × 1.3 arcsec in P.A. +63°.

that the upper limit at 8.45 GHz, 0.27 mJy, is more than 3σ away from the predicted value.

Although the discrepancy is not absurdly large, it is very unlikely that it can be accounted for by an insufficiently accurate value of the $\dot{M}/v_\infty$ ratio. The most likely explanation for the non detection is that the wind material in the outer regions, where the radio emission should form, is not ionized.

Using the results of Sect. 3.2.1 we estimated the number of Lyman photons needed to keep the wind ionized everywhere and compared it to the number of Lyman photons emitted by the star. From Eq. (5) and using model atmospheres (Kurucz 1992) we obtained $\log(N^\star_{Ly})$ = 40.9. On the other hand, using the wind parameters listed in Table 1 and Eq. (6) we got $\log(N^w_{Ly})$ = 45.2. Therefore, the non detection of HD 208501 is to be ascribed to the ionization status of the wind material.

The second case of non detection is HD 198478 (B3Ia). In this case the discrepancy between observations and prediction is less pronounced, $i.e.$ 0.27 mJy upper limit versus a predicted flux of 0.35 mJy. However, applying the same analysis as above one finds $\log(N^w_{Ly})$ = 45.4 and $\log(N^\star_{Ly})$ = 44.7, which suggests that, in this case too, the cause for the non detection is, most likely, the ionization status of the wind.

The case of HD 192639 (O7Ibf) requires only few comments. The predicted flux of 0.15 mJy is, in fact, below the 3σ upper limit of 0.24 mJy. Unfortunately we were not able to observe the object in the second run during which the signal to noise ratio was on average better than that of the September run allowing us to detect objects with fluxes lower than the one predicted for HD 192639 ($e.g.$ HD 14947).

For completeness we have calculated both the Lyman photon flux needed to keep the wind fully ionized, N^w_{Ly} (Eq. 6), and the Lyman photon flux expected from model atmospheres, $N^\star_{Ly}$ for all of the stars in our sample and the results are listed in Table 4. It is clear that the supergiants hotter than 20000 K appear to have enough Lyman continuum photons to keep the whole wind ionized (*i.e.* $N^w_{Ly} < N^\star_{Ly}$). Cooler supergiants do not show a unique behaviour. The problem arises for those stars that, according to Table 4, do not have enough Lyman photons to ionize the wind up to large distances, but, on the other hand, do show a radio emission perfectly consistent with the predictions made on the basis of their observed Hα emission, which requires the wind to be wholly ionized. In some cases the discrepancy between $\log(N^w_{Ly})$ and $\log(N^\star_{Ly})$ is marginal in that it is within the uncertainties with which the two quantities can be estimated. In other cases (namely P Cygni and Cyg OB2 12) the difference is two or three orders of magnitude. A solution to this problem has been already proposed by Felli et al (1985) in their discussion of the case of P Cygni: the missing ionizing radiation should be provided by the Balmer continuum photons. However, this cannot be the general explanation because

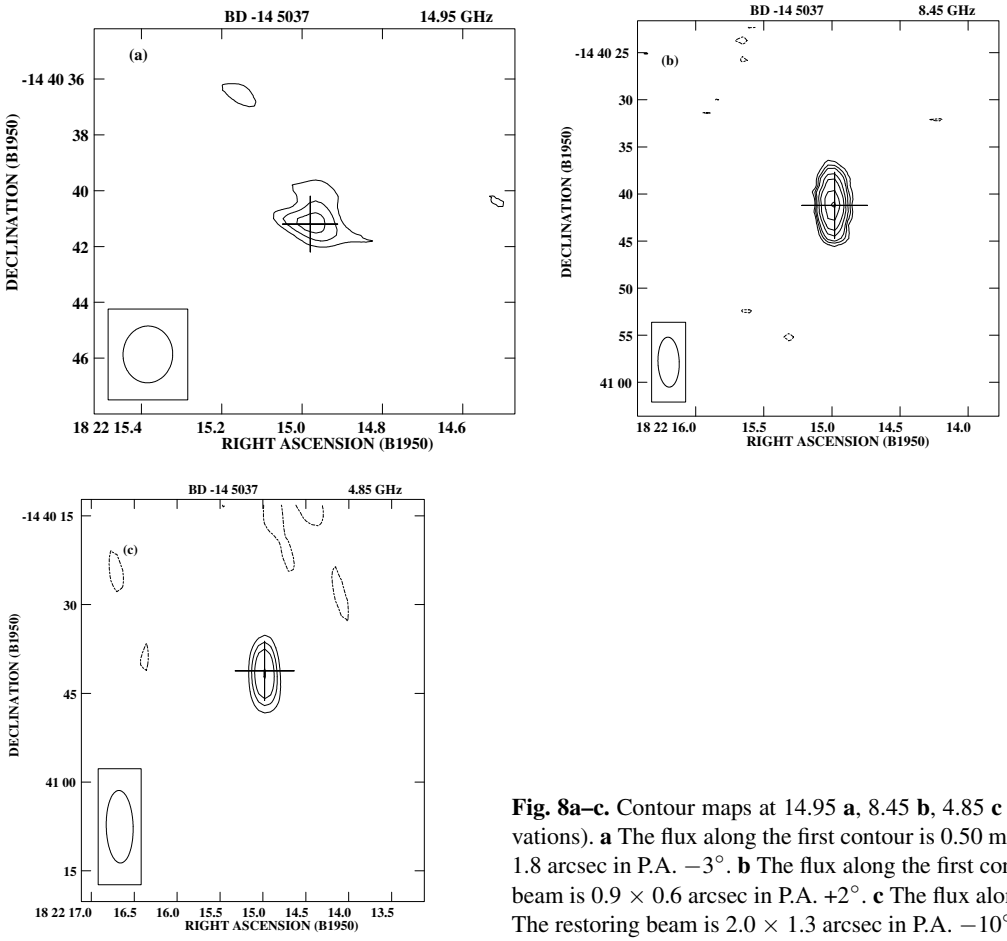

Fig. 8a–c. Contour maps at 14.95 **a**, 8.45 **b**, 4.85 **c** GHz of BD -14 5037 (october observations). **a** The flux along the first contour is 0.50 mJy/beam. The restoring beam is 2.0 × 1.8 arcsec in P.A. -3°. **b** The flux along the first contour is 0.12 mJy/beam. The restoring beam is 0.9 × 0.6 arcsec in P.A. $+2^\circ$. **c** The flux along the first contour is 0.17 mJy/beam. The restoring beam is 2.0 × 1.3 arcsec in P.A. -10°.

all B supergiants have a number of Balmer photons (in particular $\log(N^{\star}_{Balmer}) = 49 \div 51$) high enough to make the mechanism work for all of them, if present, but for some of them the radio emission is well below the expected level if they had a wind ionized entirely. It is clear that the concurrence of another, so far unidentified phenomenon (geometric effects? variability?) is needed to make it possible for Balmer continuum photons to be as efficient as to ionize the wind of a B supergiant up to large distances from the stellar surface. More observational and theoretical work is needed to clarify this point fully.

4.2. One frequency detections

HD 2905 (κ Cas) – This star had never been detected before even though it had previously been observed (BAC 1989). The measured flux is about twice as high as our predictions which would imply a mass loss rate 1.8 greater than derived from Hα (see Table 5). Either variability in the mass loss rate or non thermal contribution to the radio emission can explain the discrepancy. More observations at different frequencies are then needed to clarify this issue.

HD 14947 – This is a new detection, too. The observed flux is in this case a factor of two lower than predicted. Also in this case more observations are needed before ruling out the variability in mass loss rate as the cause for the discrepancy.

HD 190429 – This object is another new detection. We detected it at 8.45 GHz in the October run but not in the September run that is much more noisy. We put an upper limit at 4.85 GHz. The observed flux is about half the predicted one. This difference is a possible indication of variability. Indeed, Hα observations reveal that the equivalent width increased by a factor of about 2 between the 1988 and the 1991 campaigns (Scuderi 1994; Scuderi et al. 1992, Scuderi and Panagia 1997). It is clear then that further investigation is needed. Not much can be said about the thermal origin of the emission even though the 4.85 GHz upper limit is consistent with a thermal spectral index.

4.3. Two frequency detections

HD 194279 – The object was detected during the September observations at 8.45 GHz and 4.85 GHz but not at 14.95 GHz, whereas during the October run was reobserved at 4.85 GHz but not detected. The spectral index as computed from the 8.45 GHz and 4.85 GHz measurements is 0.81, so that the emission is of thermal origin. The observed fluxes are very close to the predicted ones and the slight differences are probably due to

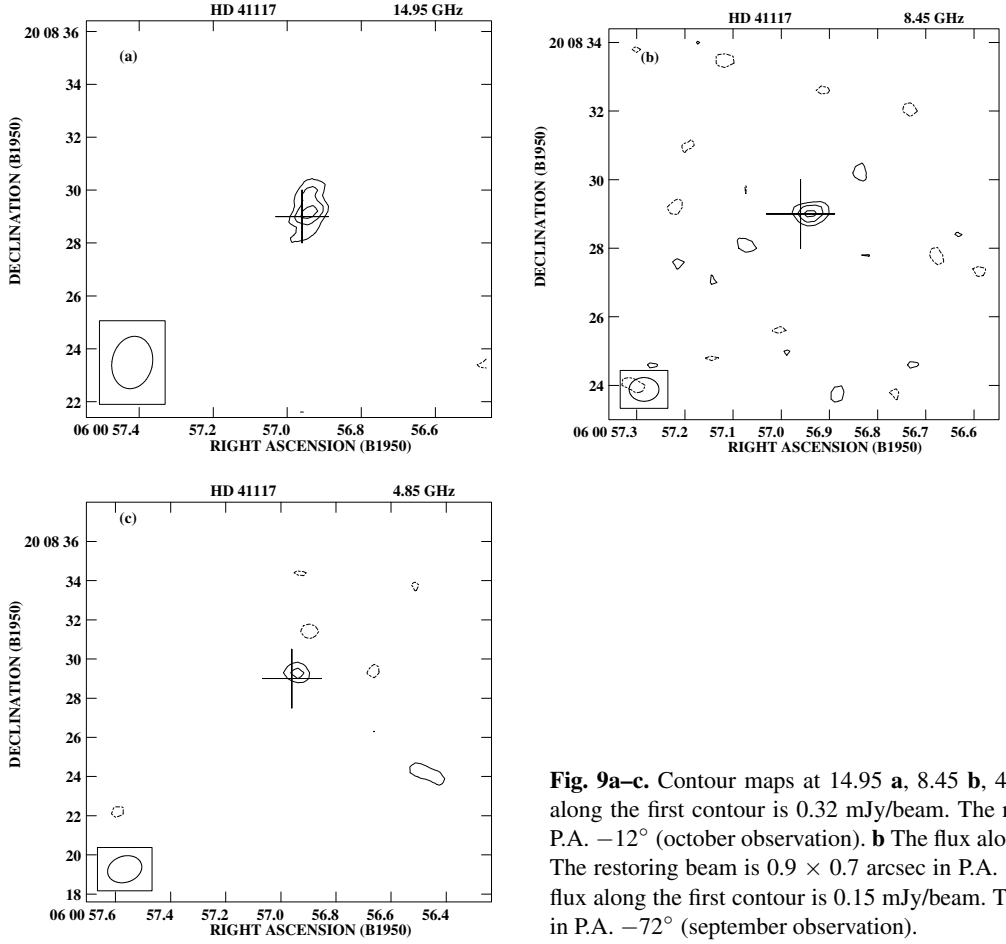

Fig. 9a–c. Contour maps at 14.95 **a**, 8.45 **b**, 4.85 **c** GHz of HD 41117. **a** The flux along the first contour is 0.32 mJy/beam. The restoring beam is 2.0 × 1.5 arcsec in P.A. -12° (october observation). **b** The flux along the first contour is 0.20 mJy/beam. The restoring beam is 0.9 × 0.7 arcsec in P.A. -90° (september observation). **c** The flux along the first contour is 0.15 mJy/beam. The restoring beam is 1.8 × 1.3 arcsec in P.A. -72° (september observation).

the value for terminal velocity of the wind which has not been measured and had to be assumed when estimating the radio flux.

4.4. Three frequency detections

HD 30614 (α Cam) – The object was detected at all frequencies. Comparison with a previous 4.85 GHz measurement (BAC 1989) shows a difference (see Table 2) which is, however, quite small (the central values of the measurements are 1σ away from each other) to be considered evidence for variability. The spectral index is 0.91±0.18 indicating a thermal origin of the emission. All the observed fluxes, though systematically smaller, agree within the errors with the predicted ones.

HD 37128 (ϵ Ori) – This object is very similar to the previous one. The 4.85 GHz measurement compared with the available data (Abbott et al. 1980) suggests the presence of variability. In fact, the 4.85 GHz measurements differs by as much as a factor of 2.5 which, even taking into account the large error in the Abbott et al. data, is very likely significant. The spectral index of the emission is α=0.73±0.16. Furthermore, there is fair agreement between the observed and Hα derived flux. For this star Scuderi (1994) measured significant variations of the Hα profile on a timescale of few hours.

HD 41117 – This star is detected for the first time at all three observed frequencies. It was observed twice at 8.45 GHz and the two measurements agree within the errors; therefore, we averaged the two values. The spectral index, α, is 0.76±0.03, and clearly shows the thermal origin of the emission. Also the agreement between predicted and observed fluxes is quite good.

HD 190603 – This star was observed at 4.85 GHz and 14.95 GHz by Abbott (1985) and Abbott et al. (1980). Our new measurements confirm the old one and add a new data point to the radio spectrum. The spectral index is rather flat (α=0.19±0.11) suggesting substantial contribution to the emission of non-thermal processes. Furthermore, the fact that the observed fluxes are all *lower* than the ones predicted from Hα, which was observed in 1990, is an indication of variability in the mass loss rate.

HD 193237 (P Cyg) – The case of *P Cygni* deserves some detailed comments. The star has been indicated for long time as a variable radio source (see for example van den Oord et al. 1985). Recently, Skinner et al. 1996 have studied this variability and found that most of it is may be due to the fact the VLA resolves the source even with its lowest spatial resolution (D configuration). Skinner et al. have combined 7 years' data and pointed out that bona fide variations in the radio flux are quite small. Nevertheless they observed some short lived and large amplitude variations whose interpretation is still a problem. The average radio fluxes measured by Skinner et al. 1996 at 4.85 and 14.95 GHz are 10 mJy and 20 mJy, respectively. The differences

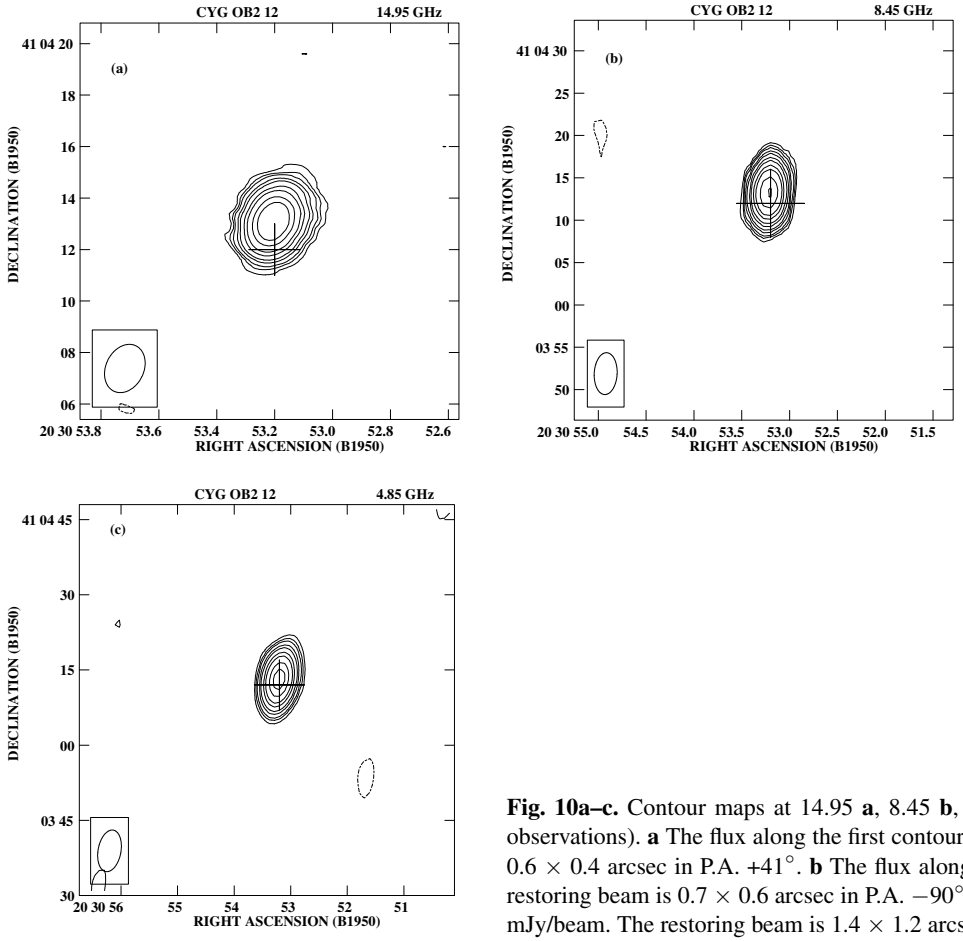

Fig. 10a–c. Contour maps at 14.95 **a**, 8.45 **b**, 4.85 **c** GHz of Cyg OB2 12 (september observations). **a** The flux along the first contour is 0.75 mJy/beam. The restoring beam is 0.6×0.4 arcsec in P.A. $+41^\circ$. **b** The flux along the first contour is 0.35 mJy/beam. The restoring beam is 0.7×0.6 arcsec in P.A. -90°. **c** The flux along the first contour is 0.50 mJy/beam. The restoring beam is 1.4×1.2 arcsec in P.A. $+29^\circ$.

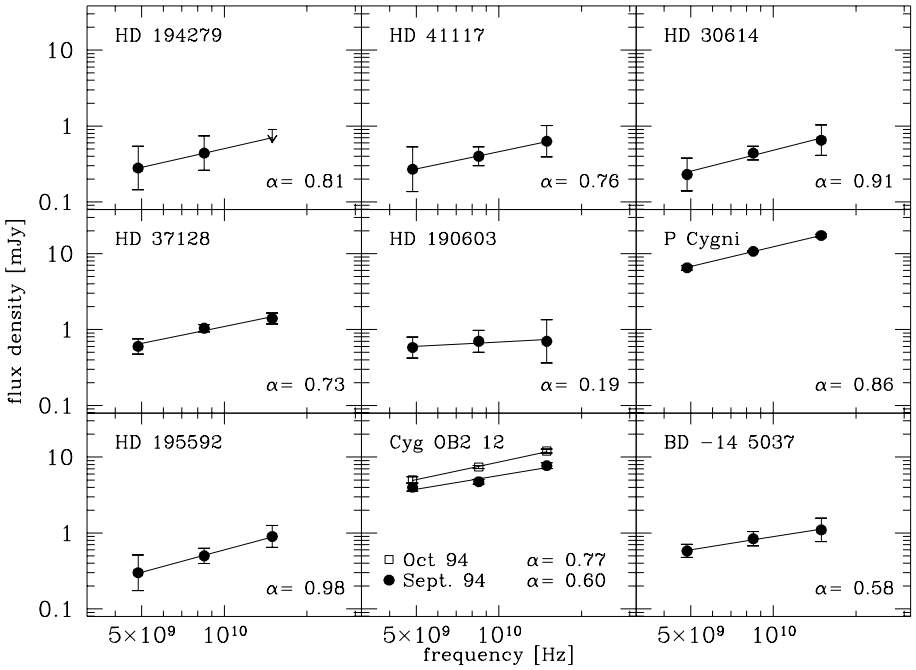

Fig. 11. The averaged radio spectra of the sources detected at least at two frequencies. The two measurements of Cyg OB2 12 have not been averaged.

Table 3. Observations

Object	Date of observation	Integration Time [m] 14.95 [GHz]	8.45 [GHz]	4.85	Flux density [mJy] 14.95 [GHz]	8.45 [GHz]	4.85
HD 190429	Sept. 1994	–	20	20	–	<0.27	<0.21
	Oct. 1994	–	40	–	–	0.28 (0.03)	–
HD 14947	Sept. 1994	–	40	–	–	<0.27	–
	Oct. 1994	–	40	–	–	0.11 (0.03)	–
HD 192639	Sept. 1994	–	40	–	–	<0.24	–
HD 30614 – $\alpha\ Cam$	Oct. 1994	20	20	20	0.65 (0.13)	0.44 (0.04)	0.23 (0.05)
HD 195592	Sept. 1994	–	20	30	–	0.42 (0.10)	0.27 (0.07)
	Oct. 1994	20	20	30	0.90 (0.13)	0.53 (0.04)	0.30 (0.07)
HD 37128 – $\epsilon\ Ori$	Oct. 1994	20	20	20	1.40 (0.10)	1.04 (0.04)	0.60 (0.06)
HD 2905 – $\kappa\ Cas$	Oct. 1994	–	40	–	–	0.40 (0.03)	—
HD 193237 – $P\ Cyg$	Oct. 1994	5	5	5	17.3 (0.30)	10.7 (0.07)	6.50 (0.20)
HD 190603	Sept. 1994	15	10	10	0.70 (0.20)	0.70 (0.10)	0.58 (0.06)
HD 194279	Sept. 1994	20	20	20	<0.90	0.44 (0.10)	0.28 (0.08)
	Oct. 1994	–	–	20	–	–	<0.36
BD –14 5037	Sept. 1994	–	20	30	–	0.72 (0.08)	0.63 (0.05)
	Oct. 1994	20	20	20	1.10 (0.20)	0.97 (0.05)	0.53 (0.07)
HD 41117	Sept. 1994	–	20	20	–	0.44 (0.08)	0.27 (0.06)
	Oct. 1994	20	20	–	0.63 (0.13)	0.38 (0.04)	–
HD 198478	Sept. 1994	–	20	20	–	<0.27	<0.15
Cyg OB2 12	Sept. 1994	5	5	5	7.70 (0.30)	4.74 (0.14)	4.00 (0.20)
	Oct. 1994	5	5	5	12.0 (0.20)	7.40 (0.08)	5.03 (0.10)
HD 208501	Sept. 1994	–	20	20	–	<0.27	<0.24

[1] The values in parenthesis are the $r.m.s.$ noises measured on the radio images. The errors on the flux densities can be calculated using the formula given in Sect. 2.2.

Table 4. Results

Object	ST	$\dot{M}$(Hα) $[10^{-6} M_{\odot} yr^{-1}]$	$\dot{M}$(Radio) $[10^{-6} M_{\odot} yr^{-1}]$	α	log(N^{w}_{Ly})	log($N^{\star}_{Ly}$)
HD 190429	O4If	7.5±1.2	4.6±0.6	–	46.8	49.6
HD 14947	O5If	5.4±1.1	3.0±0.7	–	46.7	49.3
HD 192639	O7Ibf	2.4±0.5	<3.5	–	46.3	48.8
HD 30614 – $\alpha\ Cam$	O9.5I	2.9±0.6	2.5±0.5	0.91±0.18	46.7	48.9
HD 195592	O9.5I	3.8±0.8	5.1±1.3	0.98±0.04	46.9	49.1
HD 37128 – $\epsilon\ Ori$	B0Ia	1.6±0.4	2.1±0.3	0.73±0.16	46.1	48.2
HD 2905 – $\kappa\ Cas$	B1Ia	1.1±0.2	2.0±0.3	–	45.7	46.6
HD 193237 – $P\ Cyg$	B1Ia^{+}	19.0±0.2	21.0±4.0	0.86±0.02	49.1	46.8
HD 190603	B1.5Ia^{+}	3.5±0.7	<1.7	–	47.1	46.5
HD 194279	B1.5Ia	1.5±0.3	1.2±0.3	0.81	46.3	46.3
BD -14 5037	B1.5Ia	3.4±0.7	4.4±0.9	0.58±0.06	47.1	46.6
HD 41117	B2Ia	1.6±0.3	1.5±0.2	0.76±0.03	46.1	46.2
HD 198478	B3Ia	0.5±0.1	<0.4	–	45.4	44.7
Cyg OB2 12	B5Ia	8.6±1.8	13.0±2.8	0.60±0.17	47.5	44.7
			18.0±4.1	0.77±0.05		
HD 208501	B8Ib	0.7±0.2	<0.4	–	45.2	40.9

with the fluxes in Table 2 are likely due to resolution problems, in that Skinner et al. 1996 include both the compact source and the more extended nebulosity associated with P Cyg.

In our observations the source appears to be resolved at 4.85 GHz, barely resolved at 8.45 GHz and unresolved at 14.95 GHz. The apparent paradox of a higher resolution at lower frequencies can be understood in terms of a composite source made of a compact, optically thick, source (stellar wind) embedded in a more extended, optically thin HII nebulosity. In this case, the relative importance of the extended emission decreases strongly at higher frequencies whereas the angular resolution of the radiotelescope increases. As a consequence, at high frequencies

the average flux per resolution element of the extended component becomes much fainter than the peak flux of the compact source and may effectively become undetectable. The fluxes shown in Table 4 are the peak fluxes and, as one can see, they agree quite well with the previous measurements reported in Table 2. The integrated flux at 4.85 GHz is 10.5 mJy which is very close to the average value reported by Skinner et al. 1996. Our data appear to confirm one of the conclusions of Skinner et al.,$i.e$ that the radio emission of $P\ Cygni$ is quite stable. Finally the spectral index calculated using the radio fluxes in Table 4 turned out to be 0.86±0.02.

HD 195592 – This object is one of the new detections. It is another "well behaved" object, in the sense that its spectral index, being 0.98±0.04, indicates that the emission is thermal in origin. Also the observed fluxes agree with the predicted ones rather closely.

Cyg OB2 12 – The two sets of measurements show evidence for variability. The radio flux measured during the October run is on average a factor 1.5 stronger with respect to the September measurements. Comparison with other data (BAC 1989; Contreras et al. 1996) seems to confirm this behaviour. The spectral index seems to steepen going from 0.60±0.18 to 0.77±0.05, but the variation is within the errors. The slope of the spectrum in the two epochs clearly indicates a thermal origin of the emission.

BD –14 5037 – This is another of the new detected objects. The spectral index is 0.58±0.06 so, virtually identical to the canonical value for thermal emission originating in a wind. The object was observed twice at 8.45 GHz and 5GHz and the available measurements were combined. The predicted fluxes are a factor 1.5 smaller than the observed ones. This discrepancy may be due to the value of the terminal velocity assumed for the estimate of the radio flux. In fact, adopting a somewhat lower terminal velocity, $i.e.$ 450 $km\ s^{-1}$ instead of the average 750 $km\ s^{-1}$ given by Prinja et al. (1990), would give perfect agreement. Such lower value is perfectly reasonable, as, for example, the measured v_∞ of HD 190603 shows (see Table 1).

In Fig. 11 we have reported the average radio spectra of the sources detected at least at two frequencies. The solid line is the weighted least square fit to the data.

5. Discussion

5.1. The radio emission spectral index

Fig. 12 shows the distribution of the radio spectral index, α, of the objects with three frequency detections. For Cyg OB2 12 we have used an average value between the two available epochs. As one can see there is only one object with spectral index equal to the canonical value of 0.6. All the other objects have a higher spectral index whose mean value (obtained through a weighted average) is 0.82±0.13. The spread in the distribution is within the average measurement error. The dotted histogram in Fig. 12 includes also the only other two objects for which radio measurements are available at three different frequencies (namely HD 66811 - $\zeta\ Pup$ and HD 152408, see Lamers & Leitherer 1993). As one can see they fit very well into the shaded distribution.

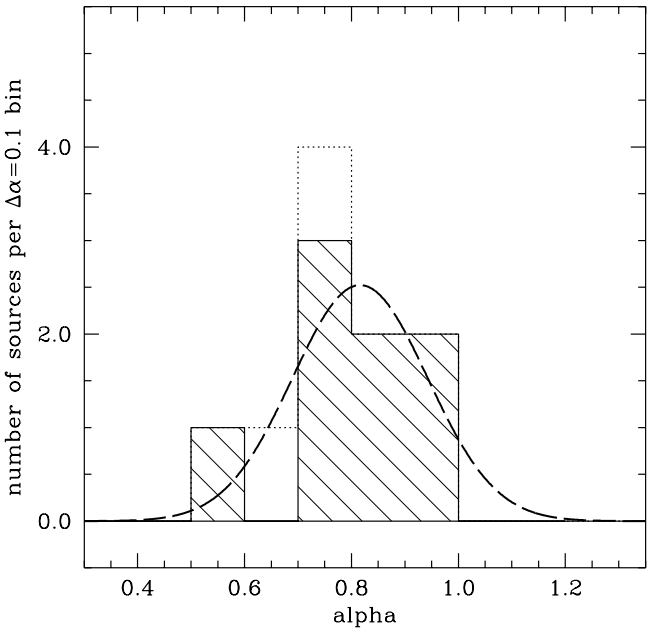

Fig. 12. Distribution of the radio spectral index, α of the objects detected at three different frequencies (shaded histogram). The dotted histogram includes two more objects from the literature.

As shown by Panagia & Felli (1975), a steeper spectrum implies a density that decreases more slowly than R^{-2} or, in turn, a wind that is decelerated at large distances from the stellar surface. In this case the appropriate expansion velocity should be lower than the so-called "terminal velocity" which is measured by the blue edge of the P Cyg line profiles. It is worth noting that a decelerated wind would produce additional absorption at intermediate velocities in the blue side of P Cyg lines. Such a possibility would help explaining relatively narrow absorptions observed in high mass loss rate stars (such as P Cyg itself, see Scuderi et al. 1994) whose presence has eluded all theoretical modelling attempts so far.

Experimentally, we do not find any systematic correlation of the spectral index with either the mass loss rate or the star spectral type. Therefore, at this stage, although it is apparent that wind deceleration at large distances is a promising possibility, we do not have any definite clue about its cause.

A steeper radio spectrum could be also produced by the presence of a temperature gradient. If the temperature decreases with the radius it is easy to show that the radio spectral index must be steeper than the canonical value 0.6 (Leitherer & Robert 1991).

5.2. Variability in the radio flux

When comparing the datasets obtained in the two runs only Cyg OB2 12 shows evidence of strong variability in the radio flux. If previous observations are considered, then also HD 37128 ($\epsilon\ Ori$) radio flux appears to have varied appreciably.

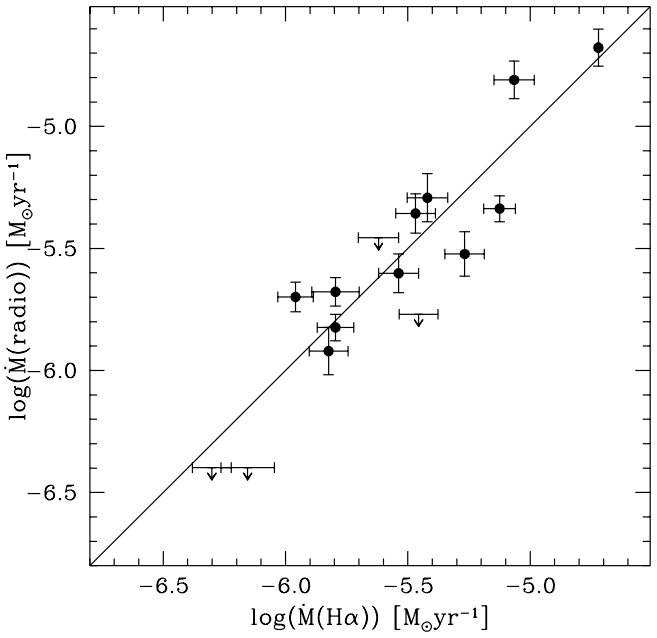

Fig. 13. The correlation between Hα derived and radio derived mass loss rate. The solid line has slope one.

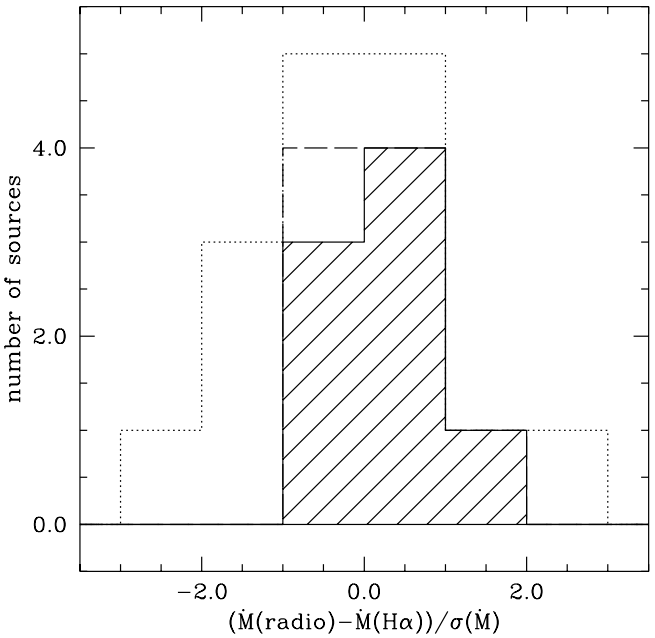

Fig. 14. The difference between radio and Hα mass loss rate in units of the measurement errors. The dotted histogram refers to all mass loss rate value including upper limits and variable sources (Cyg OB2 12). The dashed histogram includes only the detected objects. The shaded histogram included all the detected sources with thermal spectral index.

Radio variability is usually associated with non thermal emitters. However, this seems not to be the case here because both Cyg OB2 12 and HD 37128 have spectral slopes that clearly indicate the thermal origin of their emission. The variation in the mass loss rate is the most likely explanation to this phenomenon over the time scale of approximately one month that separates the two epochs.

5.3. The Hα – radio correlation

One of the aims of this study was to compare the mass loss rates obtained from the analysis of the Hα line with the ones derived from radio flux measurements for a sample of stars statistically significant.

We have determined the radio mass loss rates using Eq. (2) and the stellar and wind parameters contained in Table 1. The mean atomic weight per electron μ_e was assumed to be 1.3 for all stars with the exception of P Cyg for which we took μ_e = 2 due to the observed helium overabundance (He/H=0.5 by number, $e.g.$ Barlow 1991, Scuderi et al. 1994). We calculated a weighted mean among the mass loss rate values obtained from the measurements at different frequencies. The results are reported in Table 5 together with the Hα derived mass loss rates. The errors listed in the table were estimated taking into account the uncertainties on the measured quantities ($e.g.$ the flux radio density or the intensity of the Hα line) and that of the assumed quantities ($e.g.$ the effective temperature). Since an error in the distance would affect both the Hα and radio mass loss rates equally, as discussed in Sect. 3.1.2, no distance error has been included in the error budget.

As Table 5 and Fig. 13 clearly show the agreement between the two sets of mass loss rate values is quite good. Four objects are more than 1σ away from the relation $log(\dot{M}(radio) = log(\dot{M}(H\alpha)$ but the whole sample is within 3σ. Less than perfect estimate of the terminal velocity (in the cases when not directly measured) of the wind or variability in the mass loss could account for the remaining discrepancy. This result supports the reliability of the use of the Hα in the determination of the mass loss rate. This is particularly important because the radio method cannot be applied to stars whose emission is too low or not detectable at all because of far distance, small mass loss rate or ionization status of the wind ($e.g.$ the late B supergiants). That means that the analysis of the Hα line could be the only method to infer mass loss rates of extragalactic stars (see for example, Bianchi et al. 1994; Puls et al. 1996; and Scuderi et al. 1996).

More in detail, Fig. 14 shows the distribution of the differences between radio and Hα mass loss rates in units of the measurement errors for each source. We see that if one consider exclusively sources with no significant variability and with individually measured spectral indexes (shaded histogram in Fig. 14), the distribution is even a little narrower than expected, $i.e.$ the rms is 0.76 instead of 1. This may indicate that the error estimates are a little too conservative parameters, but may just be the result of limited statistics (only 7 sources!). The dispersion becomes appreciably larger than the errors only if one considers all sources, i.e. including also upper limits, one frequency detections (for which the radio is $assumed$ to be entirely of thermal origin) and obviously variable sources (dotted histogram of Fig. 14). We conclude that the mass loss rates determined from Hα measurements are at least as reliable as those derived from

radio measurements, with the advantage that the Hα line carries in itself all the needed information (intensity and velocity behaviour) for a correct interpretation while the radio measurements have to be complemented with (mostly UV) spectroscopic observations to have a individual measurement of the "terminal velocity" (which, as discussed above may be an overestimate of the velocity in the radio emitting region).

5.4. The mass loss rate – luminosity correlation

In Fig. 15 we have plotted the radio mass loss rate versus the stellar luminosity for the observed objects (solid circles). Since the mass loss rate and the luminosity have similar dependence in the distance ($\dot{M} \propto d^{3/2}$, $L \propto d^2$) the error bars shown in the plot do not take into account the uncertainty on the distance. The solid line is the weighted least squares fit to the observed points. The fit gives $\log \dot{M} = (1.25 \pm 0.30) \log L$ which is flatter than usually reported in literature (~ 1.6 see for example Lamers & Leitherer 1993). In Fig. 15 we also show the mass loss rates of all the other supergiants with definite or probable thermal emission we could find in literature (Lamers & Leitherer 1993, Leitherer, Chapman, & Koribalski, 1995, Persi et al. 1988, Abbott 1985). Including all points, i.e. ours plus those from the literature, a least squares fit (dotted line) yields $\log \dot{M} \propto (1.15 \pm 0.2) \log L$. It must be noted that if one considers only supergiant stars, when calculating the slope of the $\dot{M} - L$ correlation, one always finds a flatter slope than it is found with a best fit of data for stars of different luminosity classes. In fact, using the data from Lamers & Leitherer (1993) compilation and selecting only supergiants, one finds $\log \dot{M} \propto (1.3 \pm 0.2) \log L$ instead of the slope ~ 1.6 obtained for their whole sample. This result is an indication that there is a second parameter which, in addition to the luminosity, enters to determine the mass loss rates of early type stars of different luminosity classes. This aspect is discussed in more detail in Scuderi (1994) and Scuderi and Panagia (1997).

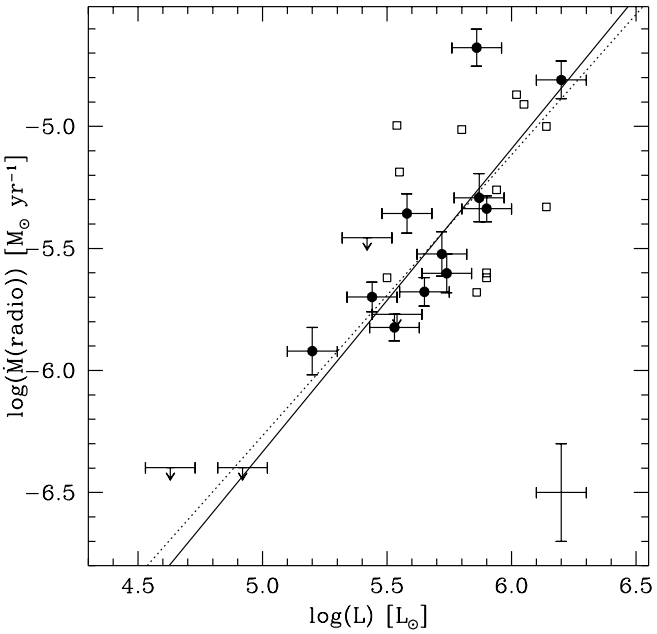

Fig. 15. The correlation between mass loss rate and the luminosity. The solid line is the linear fit to the 12 detections (solid circle). Open circle are mass loss rate derived from radio observations obtained from the literature. The dotted line is the fit to all points. The cross on the lower right corner is the assumed error for the objects from the literature.

6. Conclusions

We have searched for radio continuum emission from a sample of 15 O and B type supergiants selected from our ongoing Hα spectroscopic survey.

We detected 12 sources, out of which 7 were detected for the first time. The radio emission turned out to be of thermal origin for all objects detected at least at two frequencies but one.

We have compared the radio derived mass loss rates to the ones derived through the analysis of the Hα line. Overall, we found good agreement between the two methods. This result strongly argues in favour of the use of the Hα for mass loss rate determinations, especially for distant stars or stars with mass loss rates too low to produce appreciable radio emission.

The differences between radio and Hα determinations are slightly greater than what is accountable by errors alone. We have identified cases of incomplete ionization of the wind (2 B type supergiants) and cases of variability in the wind properties (ϵ Ori and Cyg OB2 12). These effect are enough to account for the deviations between radio and Hα mass loss determinations. Therefore, other effects, such as deviations from spherical symmetry and/or clumping, are smaller than the average errors, say, $< 20\%$.

The relationship $\dot{M} - L$ for O and B supergiants turns out to be appreciably flatter than commonly reported, *i.e.* $\log \dot{M} = (1.25 \pm 0.30) \log L$, suggesting the possibility of the existence of a second parameter on which the mass loss rate depends.

Finally our observations of the radio emission from the LBV prototype $P\ Cygni$ show that the source is quite stable. Its spectral is 0.86±0.02 clearly indicating the thermal origin of the emission and possible deceleration at large radii. This effect appears to be present in 7 out of 8 multifrequency detected stars, with clearly thermal spectral index, in our sample.

In the future we plan to complete and possibly extend our Hα survey which will provide new candidates for radio studies of mass loss rate variability.

Acknowledgements. We thank an anonymous referee for comments that helped improving the presentation of this paper.

References

Abbott, D.C., 1982, ApJ, 263, 723.
Abbott, D.C., 1985, in "Radio Stars", eds. R.M. Hjellming and D.M. Gibson, D. Reidel Publishing Company, p. 61.
Abbott, D.C., Bieging, J.H., Churchwell, E.B., & Cassinelli, J.P., 1980, ApJ, 238, 196.
Baars, J.W.M., Genzel, R., Pauliny–Toth, I.I.K., Witzel, A., 1977, A&A, 61, 99.
Barlow, M.J., 1991, in IAU Symp. 143, "Wolf–Rayet Stars and Interrelations with Other Massive Stars in Galaxies", 281.

Bianchi L., Lamers, H.J.G.L.M., Hutchings, J.B., Massey, P., Kudritzki, R., Herrero, A., & Lennon, D.J., 1994, A&A, 292, 213.
Bieging, J.H., Abbott, D.C., Churchwell, E.B., 1989, ApJ, 340, 518.
Castor, J.L., & Simon, T., 1983, ApJ, 265, 304.
Chlebowski, T., & Garmany, C.D., 1991, ApJ, 368, 241.
Chiosi, C., & Maeder, A., 1986, ARA&A, 24, 329.
Contreras, M.E., Rodriguez, L.F., Gomez, Y., & Velasquez, 1996, in "Radio emission from the stars and the Sun", eds. A.R. Taylor and J.M. Paredes, A.S.P. Conference Series, Vol. 93, p.29.
Cornwell, T., Braun, R., 1994, in "Synthesis Imaging in Radio Astronomy" ASP conf. ser. vol. 6, edited by R.A. Perley, F.R. Schwab and A.H. Bridle, p. 167.
Ebbets, D., 1982, ApJ Suppl., 48, 399.
Felli, M., & Panagia, N., 1981, A&A, 102, 424.
Felli, M., Stanga, R., Oliva, E., & Panagia, N., 1985, A&A, 151, 27.
Garmany, C.D., & Stencel, R.E., 1992, A&ASS, 94, 211.
Howarth,I.D., & Brown, A.B., 1991, IAU Symp. 143, 315.
Humphreys, R.M., 1978, ApJ Suppl., 38, 309.
Klein, R.I., & Castor, J.I., 1978, ApJ, 220, 902.
Kurucz, R.L., 1992, in IAU Symp. 149, "The Stellar Population of Galaxies", ed. B. Barbuy & A. Renzini, (Dordrecht:Kluwer), 225.
Lamers, H.J.G.L.M., 1988, in "Mass Outflows from Stars and Galactic Nuclei", eds. L. Bianchi & R. Gilmozzi, Kluwer Academic Publisher, p. 39.
Lamers, H.J.G.L.M., & Leitherer C., 1993, ApJ, 412, 771.
Lamers, H.J.G.L.M., Korevaar, P., & Cassatella, A., 1985, A&A, 149, 29.
Leitherer C., 1988, ApJ, 326, 356.
Leitherer C., Robert C., 1992, ApJ, 377, 629.
Leitherer C., Robert C., Drissen L., 1992, ApJ, 401, 596.
Leitherer C., Chapman, J.M., Koribalski, B., 1995, ApJ, 450, 289.
Olson, G.L., & Ebbets, D., 1981, ApJ, 248, 1021.
van den Oord, G.H.J. et al., 1985, in "Radio Stars", eds. R.M. Hjellming and D.M. Gibson, D. Reidel Publishing Company, p. 111.
Panagia, N., 1991, in "The physics of star formation and early star evolution", eds. C.J. Lada & N.D. Kylafis, Kluwer Academic Publishers, p. 565.
Panagia, N., & Felli, M., 1975, A&A, 39, 1.
Persi P., Ferrari-Toniolo, M., Grasdalen, G.L., 1988, in "Mass outflows from stars and galactic nuclei", eds. L. Bianchi & R. Gilmozzi, Kluwer Academic Publishers, p. 227.
Prinja, R.K., Barlow, M.J., Howarth, I.D., 1990, ApJ, 361, 607.
Puls, J., et al., 1996, A&A, 305, 171.
Reynolds, S.P., 1986, ApJ, 304, 713.
Schmid-Burgk, J., 1982, A&A, 108, 169.
Schmidt–Kaler, T., 1982, in Landolt–Bornstein, New Series: Astromony and Astrophysics, Vol. 2b (Berlin: Springer–Verlag).
Scuderi, S., 1994, PhD Thesis, University of Catania.
Scuderi, S., Bonanno, G., Di Benedetto, R., Spadaro, D., Panagia, N. 1992, ApJ, 392, 201.
Scuderi, S., Bonanno, G., Spadaro, D., Panagia, N. Lamers, H.J.G.L.M., De Koter, A. 1994, ApJ, 437, 465.
Scuderi, S., Panagia, N., Gilmozzi, R., Challis, P.M., Kirshner, R.P., 1996, ApJ, 465, 956.
Scuderi, S., Panagia, 1997, in preparation.
Simon, M., Felli, M., Cassar, L., Fischer, J., & Massi, M., 1983, ApJ, 266, 623.
Skinner, C.J., White, R.L., Becker, R.H., Barlow, M.J., Exter, K.M., Davis, R.J., Pavelin, P.E., & Bode, M.F., 1996, in, "Radio emission from the stars and the Sun", eds. A.R. Taylor and J.M. Paredes, A.S.P. Conference Series, Vol. 93, p.23.
White, R.L., 1985, ApJ, 289, 698.
Wright, A.E., & Barlow, M.J. 1975, MNRAS, 170, 41.

This article was processed by the author using Springer-Verlag LaTeX A&A style file *L-AA* version 3.